Geol. Mag. **146** (*4*), *2009, pp. 540–551. © 2008 Cambridge University Press*
doi:10.1017/S0016756808005530 *Printed in the United Kingdom*

Geochemistry of Middle Triassic gabbros from northern Liaoning, North China: origin and tectonic implications

XIAOHUI ZHANG*†, HONGFU ZHANG*, MINGGUO ZHAI*, SIMON A. WILDE‡ &LIEWEN XIE*

*State Key Laboratory of Lithospheric Evolution, Institute of Geology and Geophysics, Chinese Academy of Sciences, Beijing 100029, China
‡Department of Applied Geology, Curtin University of Technology, Perth WA, Australia

(*Received* 31 March 2008; *accepted* 16 June 2008; First published online 17 October 2008)

Abstract – The Xiaofangshen mafic stock is a hornblende gabbroic body emplaced in the Faku dome of northern Liaoning within the continental interior of the North China–Mongolian plate. Zircon U–Pb SHRIMP dating yields an emplacement age of 241 ± 6 Ma. These gabbroic rocks exhibit strong enrichment in large ion lithophile elements (e.g. Th, U) and light REE, slightly negative Eu anomalies, and pronounced depletion in high field strength elements (e.g. Nb, Ta, Zr, Ti). They show a relatively narrow range of isotopic compositions with initial $^{87}Sr/^{86}Sr$ ratios of 0.7053 to 0.7055, $\varepsilon_{Nd}(t)$ values of +0.40 to +0.68 and zircon $\varepsilon_{Hf}(T)$ values from +5.0 to +7.4. These geochemical features suggest that they might have been derived from partial melting of a subduction-related metasomatized lithospheric mantle source, which is tectonically affiliated to the Xing-Meng orogenic belt. Combined with our previous geochronological dating on the predominantly granitic intrusions from the Faku dome, it is inferred that the northern Liaoning block has a tectonic affinity with the Phanerozoic accretionary orogenic belt. This revelation further leads to the proposition that the Chifeng–Kaiyuan fault likely represents the Mesozoic lithospheric boundary between the North China craton and the Xing-Meng orogenic belt in northern Liaoning. The Xiaofangshen gabbros, together with the Triassic mafic–ultramafic cumulates and granulite xenoliths and the Triassic alkaline intrusions within the continental interior of the newly amalgamated North China–Mongolian Plate, constitute an important post-orogenic to within-plate anorogenic magmatic province, in response to the continued magmatic underplating caused by lithospheric delamination and hot asthenosphere upwelling.

Keywords: gabbro, geochemistry, origin, post-orogenic magmatism, North China.

1. Introduction

Post-orogenic mafic magmatism is one of the common features of many orogens around the world (Bonin, 2004), and may indicate that the orogen is in the process of collapsing (Dewey, 1988). The origin of such melts is commonly attributed to lithospheric extension by orogenic collapse (Ruppel, 1995), slab break-off (Davies & von Blanckenburg, 1995), convective thinning (England & Houseman, 1989), delamination of continental lithosphere (Bird, 1979; Kay & Kay, 1993) and magmatic underplating (Furlong & Fountain, 1986). Therefore, petrogenetic studies of post-orogenic mafic igneous rocks not only allow the evaluation of its mantle source, but also provide important constraints for understanding the tectonic evolution of the orogenic belts and adjacent regions.

The Faku dome in northern Liaoning occupies a transitional tectonic position that links a northern Phanerozoic orogen, that is, the Xing-Meng orogenic belt, with a southern Precambrian craton, that is, the North China craton. Based on the notion that the migmatites and metamorphic complexes from the Faku area are of a Proterozoic age (Liaoning Bureau of Geology and Mineral Resources, 1989), the Faku dome has long been regarded as a Precambrian terrane along the northern margin of the North China craton. The 1:50 000 scale geological mapping (Liaoning Bureau of Geology and Mineral Resources, 1998) and our $^{40}Ar/^{39}Ar$ geochronological study (Zhang, Wang & Li, 2005) revealed that these deformed and metamorphosed complexes, with a variety of protoliths of plutonic intrusions and supracrustal volcanic and sedimentary rocks, were genetically related to later Triassic ductile shearing events. Our zircon U–Pb SHRIMP dating further recognized that the previously established Proterozoic migmatites were in fact syntectonic granitic intrusions that were emplaced during Permian times (Zhang, Su & Wang, 2005).

In this paper, we present zircon U–Pb ages, major and trace element geochemistry, and Sr–Nd–Hf isotopic compositions for a middle Triassic mafic pluton from the Faku dome to: (1) document the geochemical characteristics of these rocks, (2) investigate their mantle sources and petrogenesis and (3) evaluate the nature of the lithospheric mantle beneath the northern Liaoning block and its tectonic affinity.

2. Geological setting

The North China craton is known as one of the world's oldest cratons, as evidenced by the presence of 3.6 Ga

†Author for correspondence: zhangxh@mail.iggcas.ac.cn

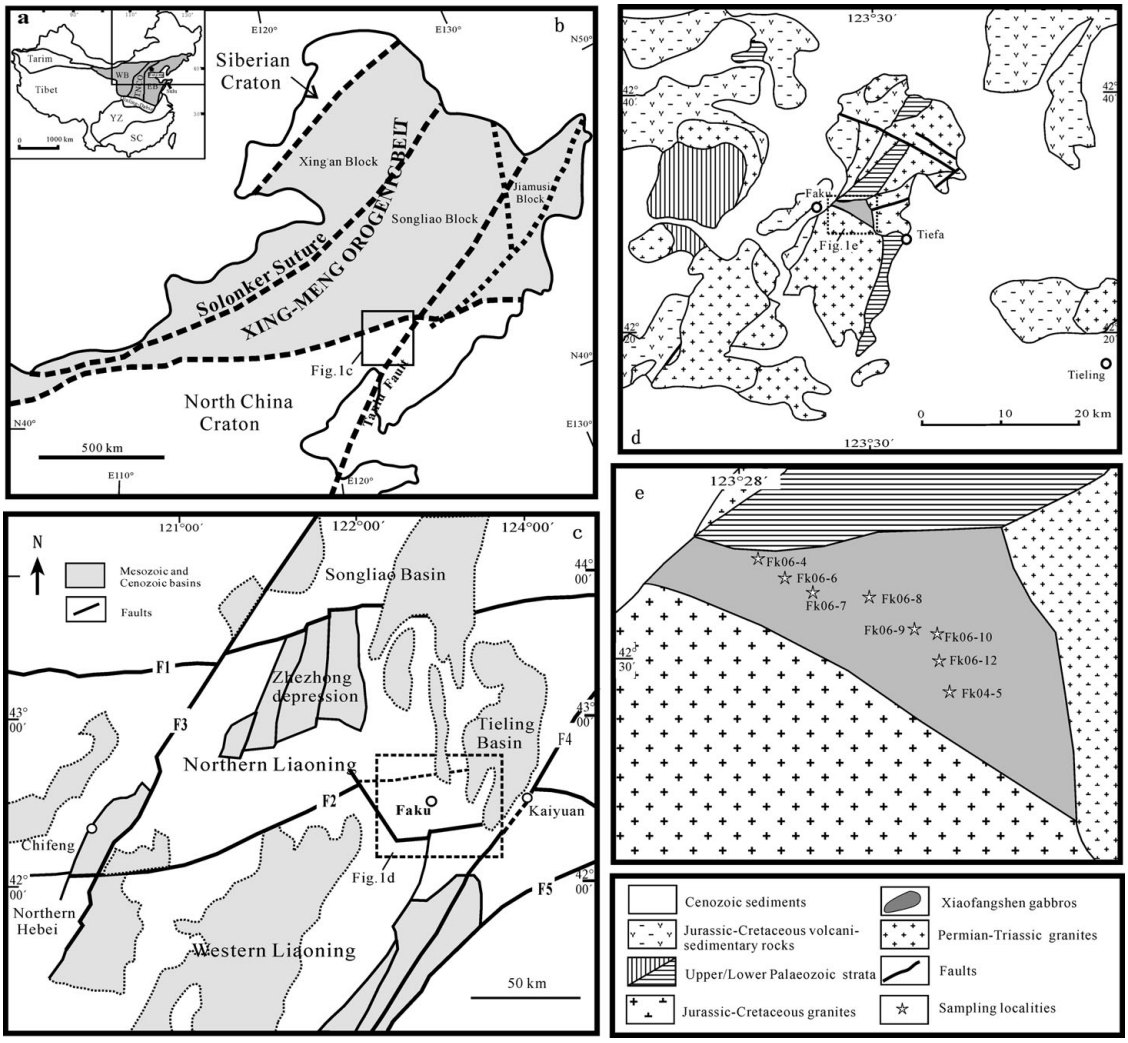

Figure 1. (a) Major tectonic divisions of China, where YZ and SC denote the Yangtze craton and South China orogen. Also shown are the subdivisions of the North China craton (Zhao *et al.* 2001), where EB, TNCO and WB denote the Eastern block, Trans-North China orogen and Western block, respectively. (b) Tectonic framework of northeastern China (modified from Gu *et al.* 2007). (c) Sketch distribution map of the basins and faults in western Liaoning, northern Liaoning and southern Songliao areas (modified from Xu *et al.* 2000); F1 – Xilamulunhe fault; F2 – Chifeng–Kaiyuan fault; F3 – Hongshan–Balihan fault; F4 – Yilan–Yitong fault; F5 – Fushun fault. (d) Sketch geological map of the Faku area (modified from Liaoning Bureau of Geology and Mineral Resources, 1998), (e) Sketch geological map of the Xiaofangshen gabbroic stock, with the sample locations shown.

crustal remnants exposed at the surface or in the lower crustal xenoliths (Liu *et al.* 1992; Zheng *et al.* 2004). It is bounded on the south by the Palaeozoic to Triassic Qinling–Dabie–Sulu orogenic belt (Meng & Zhang, 2000) and on the north by the Xing-Meng orogenic belt (Davis *et al.* 2001). The craton consists of two Archaean continental blocks, namely, the Eastern and the Western, separated by a Proterozoic orogenic belt (Fig. 1a; Zhao *et al.* 2001).

Unlike other Archaean cratons, the North China craton experienced widespread tectonothermal reactivation during and after Palaeozoic times, mainly due to the compound evolutionary history of the circum-cratonic orogenic belts. To the north, the Xing-Meng orogenic belt, also called the Altaid Tectonic Collage (Şengör, Natal'in & Burtman, 1993) or Central Asian Orogenic Belt (Jahn, Wu & Chen, 2000), is located between the North China and Siberian cratons (Fig. 1b). It is a complex orogenic belt formed through successive accretion of arc complexes, accompanied by emplacement of voluminous subduction zone granitic magmas mainly during Palaeozoic times (Davis *et al.* 2001; Xiao *et al.* 2003). During this period, multiple Mongolian arc terranes were amalgamated to the active margins of the North China craton (Davis *et al.* 2001). The Solonker suture marks the closure of the palaeo-Asian ocean and the collision between the North China craton and Mongolian composite terranes (e.g. Yin & Nie, 1996; Davis *et al.* 2001; Xiao *et al.* 2003). With the gradual exhaustion of the palaeo-Asian ocean realm, the North China craton and the southern Mongolia terranes were amalgamated and behaved as a combined North China–Mongolian plate (Davis *et al.* 2001).

Palaeozoic northeast China is the eastern segment of the Xing-Ming orogenic belt, and it is composed of three microcontinental blocks: the Jiamusi in the

southeast, Songliao in the middle and the Xing'an in the northwest (Fig. 1b). The Songliao block is composed of the Songliao Basin and the Zhangguangcai Range. The Songliao basin developed in late Mesozoic times and is an important centre for the oil industry in China.

Located to the south of the Songliao block, the northern Liaoning block mainly consists of three tectonic units: the Zhezhong depression in the west, the Faku dome in the middle and the Tieling depression in the east (Fig. 1c). The Faku dome is mainly composed of igneous and sedimentary rocks metamorphosed to greenschist- to upper amphibolite-facies grade. These rocks have been previously regarded as the Precambrian basement of the North China craton (Liaoning Bureau of Geology and Mineral Resources, 1989). The l:50 000 scale geological mapping (Liaoning Bureau of Geology and Mineral Resources, 1998) revealed that these so-called basement complexes turned out to be Phanerozoic deformed intrusions and metavolcanic and sedimentary rocks. The latter can be further divided into the lower and upper Palaeozoic formations (Fig. 1d). Our zircon U–Pb SHRIMP dating established that the majority of the granitic intrusions were emplaced during Permian times (Zhang, Su & Wang, 2005).

Since Mesozoic times, the northern Liaoning block has become part of the eastern China active tectonic belt, which experienced geodynamic transition from the palaeo-Asian to palaeo-Pacific tectonic realms. Subsequently, a series of NE- to NNE-trending strike-slip faults developed. In the Cretaceous period, the area underwent large-scale continental extension, resulting in the development of a number of basins (Xu *et al.* 2000).

3. Petrography

The Xiaofangshen gabbros, named after Xiaofangshen village, crop out as small stocks and dykes within the Permian Shijianfang granitoid batholith (Fig. 1e). The gabbros are medium- to coarse-grained rocks with intergranular textures, and show clear intrusive relations with the host granitoids. Typical samples mainly consist of plagioclase (25–70 %), amphibole (25–40 %), pyroxene (5–15 %) and biotite (0–5 %), with minor amounts of quartz, magnetite, zircon and apatite. Amphibole, the most abundant mafic mineral, mainly occurs as subhedral to euhedral phenocrysts and is locally altered to calcite and chlorite. All amphiboles belong to the calcic group (Ca+Na 1 and Na < 0.5), according to the classification of Leake *et al.* (1997) and can be classified as magnesiohastingsite, magnesiohornblende and actinolite. The plagioclase also occurs as phenocrysts; they are generally subhedral laths, with occasional albite and carlsbad–albite combined twinning and they range in anorthite content from An_{39} to An_{64}. They are partly altered to sericite, calcite and epidote.

4. Analytical methods

4.a. Zircon U–Pb isotopic dating

Zircon grains, together with standard CZ3, were cast in an epoxy mount, which was then polished to section the crystals in half for analysis. Cathodoluminescence images were obtained for the zircons prior to analysis, using a JXA-8100 microprobe at the Institute of Geology and Geophysics, Chinese Academy of Sciences, to reveal their internal structures. Measurements of U, Th and Pb were conducted using the SHRIMP II ion microprobe at Curtin University of Technology under standard operating conditions (6-scan cycle, 2 nA primary O_2^- beam, mass resolution $\sim$ 5000), following analytical procedures as described by Williams (1998). Data were processed using the SQUID (1.02) and ISOPLOT (Ludwig, 2001) programs. Corrections of Pb/U ratios were made by normalization to zircon standard CZ3 ($^{206}Pb/^{238}Pb = 0.0914$, corresponding to an age of 564 Ma). The data were corrected for common lead using the measured ^{204}Pb. Uncertainties on individual analyses are reported at the 1σ level based on counting statistics, while pooled ages are quoted at the 95 % (2σ) level.

4.b. Major and trace element determination

Both major oxides and trace element compositions were measured by a Phillips PW 2400 X-ray fluorescence spectrometer using fused glass discs and a VG-PQII ICP-MS, respectively, at the Institute of Geology and Geophysics. Analytical uncertainty (2σ) is estimated to be about $\pm$ 5 % for trace elements with abundances 10 ppm, and about $\pm$ 10 % for those 10 ppm.

4.c. Sr–Nd isotopic analyses

Sr and Nd isotopic compositions were measured on a Finnigan Mat 262 thermal ionization mass spectrometer at the Institute of Geology and Geophysics, following the procedure described in Zhang *et al.* (2008*c*). Procedural blanks were < 100 pg for Sm and Nd and < 500 pg for Rb and Sr. $^{143}Nd/^{144}Nd$ values were corrected for mass fractionation by normalization to $^{143}Nd/^{144}Nd = 0.7219$, and $^{87}Sr/^{86}Sr$ ratios normalized to $^{87}Sr/^{86}Sr = 0.1194$. Typical within-run precisions (2σ) for Sr and Nd were estimated to be 0.00002 and 0.000015, respectively. The measured values for the La Jolla Nd standard and NBS-607 Sr standard were $^{143}Nd/^{144}Nd = 0.5111853$ and $^{87}Sr/^{86}Sr = 1.20042$ during the period of data acquisition.

4.d. *In situ* Hf isotopic analyses

In situ zircon Hf isotopic analyses were conducted using the Neptune MC-ICP-MS, equipped with a 193 nm laser at the Institute of Geology and Geophysics. During analyses, the $^{176}Hf/^{177}Hf$ and $^{176}Lu/^{177}Hf$ ratios of the standard zircon (91500) were 0.282270 ± 0.000023 (2rn, n = 15) and 0.00028, similar to the commonly accepted $^{176}Hf/^{177}Hf$ ratio of 0.282284 ± 0.000003 (1r)

Table 1. SHRIMP U–Pb zircon data for the Xiaofangshen gabbros (sample Fk04-5)

Spot	U (ppm)	Th (ppm)	Th/U	Pb (ppm)	$f_{206\,(\%)}$[1]	$^{207}Pb/^{206}Pb$ (± %error 1σ)	$^{206}Pb/^{238}U$ (± %error 1σ)	$^{207}Pb/^{235}U$ (± %error 1σ)	Error correlation	Age (Ma) ^{206}Pb–^{238}U ±1σ
FK5-1	205	104	0.53	6.7	0.01	0.0522 ± 4	0.0383 ± 2	0.280 ± 4	0.382	242 ± 4
FK5-2	183	33	0.19	6.0	0.07	0.0520 ± 4	0.0379 ± 1	0.270 ± 4	0.348	240 ± 3
FK5-3	894	530	0.61	29.6	0.02	0.0500 ± 2	0.0385 ± 1	0.270 ± 3	0.614	244 ± 3
FK5-4	292	129	0.46	9.7	0.37	0.0504 ± 4	0.0386 ± 1	0.270 ± 3	0.304	244 ± 3
FK5-5	203	125	0.64	6.6	0.48	0.0465 ± 6	0.0379 ± 1	0.240 ± 5	0.254	240 ± 3
FK5-6	223	130	0.60	7.5	0.79	0.0467 ± 7	0.0387 ± 2	0.250 ± 8	0.193	245 ± 4
FK5-7	445	267	0.62	15.1	0.19	0.0494 ± 4	0.0395 ± 1	0.270 ± 4	0.348	249 ± 3
FK5-8	702	290	0.43	23.5	0.29	0.0488 ± 3	0.0388 ± 1	0.260 ± 3	0.450	245 ± 3

[1] f_{206} = percentage of common ^{206}Pb in the total measured ^{206}Pb.

measured using the solution method (Woodhead *et al.* 2004).

We have used a decay constant for $\lambda_{Lu} = 1.867\ 10^{-11}$ year^{-1} (Soderlund *et al.* 2004) and the $^{176}Hf/^{177}Hf$ and $^{176}Lu/^{177}Hf$ ratios of average chondrite and estimated depleted mantle at the present day are 0.282772 and 0.0332, and 0.28325 and 0.0384, respectively (Blichert-Toft & Albarede, 1997). These $T^{Hf}DM$ ages represent a minimum age for the source of the host magma of the zircon. We also present a more realistic estimate $T_{DM}{}^{C}$ of the age of the source rocks for the magmas, derived by projecting the initial $^{176}Hf/^{177}Hf$ of the zircon back to the depleted mantle model growth curve, assuming a mean crustal value for Lu/Hf ($^{176}Lu/^{177}Hf = 0.015$: Griffin *et al.* 2002).

5. Analytical results

5.a. Zircon U–Pb data

The SHRIMP U–Pb analysis results of the Xiaofangshen gabbro (Sample Fk04–5) are listed in Table 1. Zircons from this sample are mostly clear, euhedral to subhedral, stubby to elongate prisms (Fig. 2a). They are about 80 to 150 μm long, with length-to-width ratios between 2:1 and 4:1. Eight analyses from this sample were conducted on eight grains during a single analytical session. Measured U concentrations vary from 203 to 894 ppm, and Th ranges from 33 to 530 ppm. All analyses have Th/U ratios of 0.19–0.64 and yield a weighted mean ^{206}Pb–^{238}U age of 241 ± 6 Ma with an MSWD of 0.81 (Fig. 2b). We interpret this as the emplacement time of the Xiaofangshen gabbros.

5.b. Major oxides and trace elements

Major and trace element analyses are presented in Table 2. Samples from the Xiaofangshen pluton are mafic in composition (SiO_2 46.64–52.73 %), with high abundances of total Fe_2O_3 (7.66–13.82 %), Al_2O_3 (13.24–18.39 %) and CaO (6.35–15.28 %), low contents of TiO_2 (0.63–1.70 %) and P_2O_5 (0.08–0.47 %), and various concentrations of MgO (3.64–8.34 %) and K_2O (0.65–2.18 %). In the total alkali v. silica plot (Le Maitre, 2002) (not shown), the samples mainly plot in the field of gabbro and occasionally in the field of

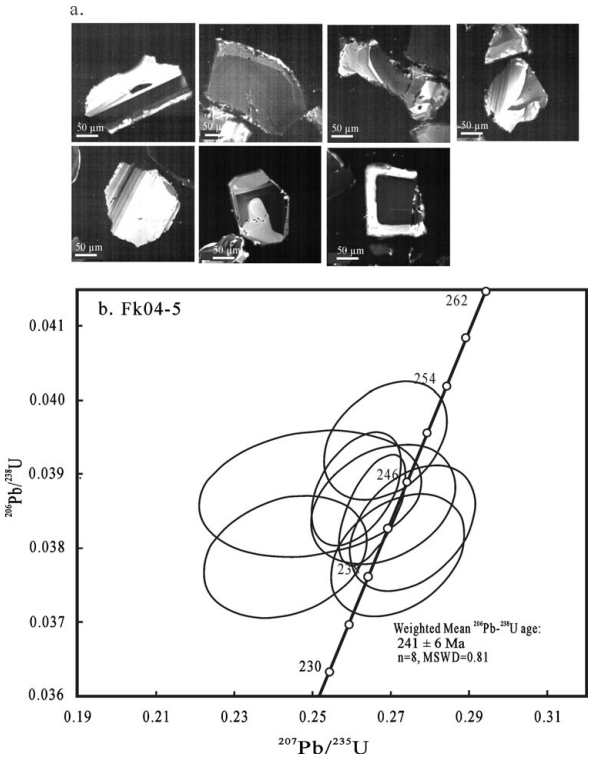

Figure 2. (a) Cathodoluminescence (CL) images of the dated zircons and (b) U–Pb zircon concordia diagrams for the Xiaofangshen gabbros.

monzodiorite. They also exhibit a transitional character between low-K tholeiitic and medium-K calc-alkaline.

In terms of trace elements, samples from the Xiaofangshen gabbros have total REE contents ranging from 70.6 ppm to 181 ppm. On the chondrite-normalized REE diagram (Fig. 3a), they display moderate light REE enrichment ($La_N/Yb_N = 4.5$ to 8.6) and small negative Eu anomalies ($Eu/Eu^* = 0.78$–0.93; Table 3). On the primitive mantle-normalized spidergram (Fig. 3b), they are enriched in large ion lithophile elements, with positive Ba, Sr, Th and U anomalies, and are depleted in high field strength elements, with pronounced negative Nb, Ta, Zr, Hf and Ti anomalies.

5.c. Whole rock Sr–Nd isotopes and zircon Hf isotopes

The results of Sr–Nd isotope analyses are given in Table 3. The initial isotopic ratios were calculated based on the age of 241 Ma. As shown in a plot of $\varepsilon_{Nd}(t)$

Table 2. Major and trace element data for the Xiaofangshen gabbros

Sample	Fk06-4		Fk06-7	Fk06-8		Fk06-10	Fk06-12	Fk04-5
Longitude	E123°28′09″		E123°28′28″	E123°28′47″		E123°29′08″	E123°29′12″	E123°29′32″
Latitude	N42°30′50″	Fk06-6	N42°30′37″	N42°30′35″	Fk06-9	N42°30′13″	N42°29′57″	N42°29′46″
SiO_2	47.26	52.73	47.40	46.64	48.17	50.24	51.72	51.42
TiO_2	1.51	1.32	1.50	1.70	1.42	1.02	0.63	0.92
Al_2O_3	14.09	18.39	16.90	14.12	15.64	16.68	15.59	13.24
TFe_2O_3	12.80	9.20	11.19	13.72	11.66	7.66	8.13	9.72
MnO	0.18	0.17	0.17	0.19	0.19	0.15	0.17	0.18
MgO	8.34	3.64	6.51	8.11	7.10	7.31	7.27	6.05
CaO	10.26	6.35	10.71	10.39	10.52	11.08	10.31	15.28
Na_2O	2.21	4.13	2.96	2.19	2.90	3.04	3.21	2.12
K_2O	1.43	2.18	1.03	1.36	1.16	1.02	1.22	0.65
P_2O5	0.19	0.47	0.18	0.18	0.09	0.08	0.26	0.14
LOI	1.15	1.68	0.97	1.28	0.87	1.03	0.98	0.22
Total	99.42	100.26	99.52	99.87	99.72	99.31	99.50	99.94
Mg no.	60.3	48.0	57.6	57.9	58.7	69.0	67.6	59.2
Sc	49.3	14.5	32.9	47.7	36.4	38.6	33.8	53.4
V	419	170	321	493	306	164	134	191
Cr	291	11.3	26.2	275	143	92.0	346	438
Co	46.4	20.6	38.5	50.3	37.5	33.1	29.8	41.6
Ni	45.6	23.3	48.8	46.1	59.5	73.0	88.4	126
Ga	17.7	20.8	20.1	18.5	20.1	17.5	18.7	13.6
Rb	46.4	65.7	20.4	39.5	22.0	23.8	31.6	14.1
Sr	487	733	772	497	683	704	715	649
Y	20.7	28.2	26.3	19.6	26.2	24.2	37.3	18.5
Zr	70.2	189	73.8	73.1	87.7	84.0	94.9	69.6
Nb	3.85	13.2	8.39	3.86	9.18	7.55	10.1	3.20
Cs	1.60	2.36	1.19	1.56	1.32	1.45	1.33	1.40
Ba	179	925	507	155	313	407	224	111
Hf	2.33	4.50	2.65	2.40	3.15	2.84	2.96	2.29
Ta	0.26	0.68	0.43	0.24	0.48	0.42	0.63	0.80
Pb	6.56	13.4	8.93	6.77	8.78	10.3	9.35	4.58
Th	3.13	2.39	1.03	3.28	1.55	1.02	2.69	2.43
U	0.92	1.12	0.38	1.22	0.55	0.34	0.83	0.74
La	15.4	33.5	21.5	14.9	21.2	18.6	31.5	10.3
Ce	30.7	68.2	48.1	28.7	48.1	41.0	68.5	26.6
Pr	4.34	8.99	6.52	4.12	6.85	5.70	9.60	3.42
Nd	18.3	34.9	26.1	17.5	27.7	23.1	36.9	13.9
Sm	4.45	7.09	5.65	4.31	5.76	5.24	7.74	3.24
Eu	1.28	2.08	1.53	1.27	1.53	1.44	1.84	1.02
Gd	4.42	6.54	5.15	4.26	5.30	4.99	6.82	3.50
Tb	0.70	0.99	0.81	0.68	0.84	0.82	1.11	0.58
Dy	4.06	5.68	4.66	3.94	4.94	4.77	6.54	3.33
Ho	0.81	1.15	0.96	0.78	1.02	0.97	1.38	0.66
Er	2.11	3.06	2.56	2.06	2.81	2.66	3.88	1.83
Tm	0.31	0.43	0.38	0.29	0.43	0.40	0.60	0.24
Yb	1.83	2.80	2.45	1.83	2.83	2.56	3.98	1.66
Lu	0.27	0.41	0.36	0.26	0.42	0.38	0.61	0.25
La_N/Yb_N	6.04	8.59	6.29	5.85	5.38	5.21	5.68	4.45
Eu/Eu*	0.88	0.93	0.87	0.91	0.85	0.86	0.78	0.93

Table 3. Rb–Sr and Sm–Nd isotopic compositions for the Xiaofangshen gabbros

Sample no.	Rb (ppm)	Sr (ppm)	$^{87}Rb/^{86}Sr$	$^{87}Sr/^{86}Sr$	$\pm2\sigma$	$(^{87}Sr/^{86}Sr)_t$	Sm	Nd	$^{147}Sm/^{144}Nd$	$^{143}Nd/^{144}Nd$	$\pm2\sigma$	Initial Nd	ε_{Nd} (t)	T_{DM} (Ma)	T_{DM2} (Ma)
FK06-4	44.47	482.9	0.2670	0.706463	42	0.705548	4.265	17.49	0.1474	0.512595	0.000013	0.512362	0.68	1275	956
FK06-8	38.70	477.4	0.2345	0.706345	14	0.705541	4.116	16.67	0.1493	0.512597	0.000013	0.512361	0.66	1307	958
FK06-9	21.09	704.8	0.0865	0.705672	13	0.705375	5.958	27.73	0.1299	0.512567	0.000011	0.512362	0.67	1060	958
FK06-10	22.66	763.1	0.0859	0.705738	14	0.705444	5.353	23.63	0.1369	0.512572	0.000014	0.512356	0.55	1146	967
FK06-12	30.22	722.4	0.1210	0.705926	14	0.705511	7.298	35.89	0.1229	0.512542	0.000013	0.512348	0.40	1020	980

Chondrite Uniform Reservoir (CHUR) values ($^{87}Rb/^{86}Sr = 0.0847$, $^{87}Sr/^{86}Sr = 0.7045$, $^{147}Sm/^{144}Nd = 0.1967$, $^{143}Nd/^{144}Nd = 0.512638$) are used for the calculation. $\lambda_{Rb} = 1.42\times10^{-11}$ year^{-1} (Steiger & Jäger, 1977); $\lambda_{SM} = 6.54\times10^{-12}$ year^{-1} (Lugmair & Harti, 1978).

v. $(^{87}Sr/^{86}Sr)_i$ (Fig. 4), the samples have a restricted range of isotopic compositions with initial $^{87}Sr/^{86}Sr$ ratios of 0.7053 to 0.7055, slightly positive $\varepsilon_{Nd}(t)$ values of +0.40 to +0.68 and model ages (T_{DM2}) of 956 to 980 Ma.

Zircons from the Xiaofangshen gabbros show a range of initial $^{176}Hf/^{177}Hf$ ratios from 0.28276 to 0.28282 and $\varepsilon_{Hf}(T)$ values from 5.0 to 7.4 (Table 4, Fig. 5). The Hf model ages (T_{DM}) for these zircons mainly range between 568 to 654 Ma.

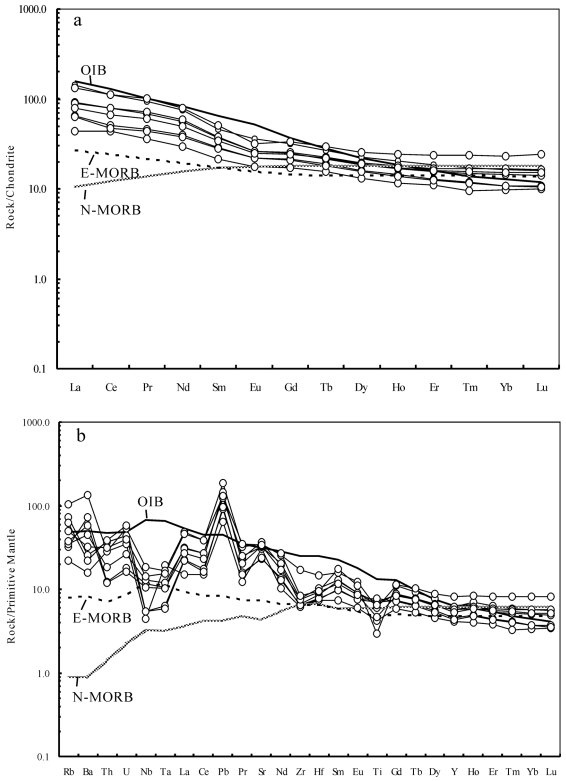

Figure 3. (a) Chondrite-normalized REE patterns and (b) primitive mantle-normalized trace element spidergrams for the Xiaofangshen gabbros. Normalization values are from Sun & McDonough (1989). The data for oceanic island basalt (OIB), normal mid-ocean ridge basalt (N-MORB) and enriched mid-ocean ridge basalt (E-MORB) are also from Sun & McDonough (1989).

6. Discussion

6.a. Petrogenesis

The low silica contents ($SiO_2 = 46.64$–52.73 wt %) and relatively high concentrations of Fe_2O_3 and MgO (7.66–12.80 wt % and 3.64–8.34 wt %, respectively) of the Xiaofangshen gabbros, and high Cr contents (275–438 ppm) in some samples, suggest that they were derived from a mantle source. Nevertheless, their moderate Mg no. (48.0–67.6) and low Ni concentrations (23–126 ppm) indicate that they do not represent primary magmas, but may have experienced some crystal fractionation, most likely of olivine and clinopyroxene, as reflected by the Cr–Ni fractionation vector plot (Fig. 6a) and the negative relationship between Cr and Y (excluding sample Fk06–12) (Fig. 6b).

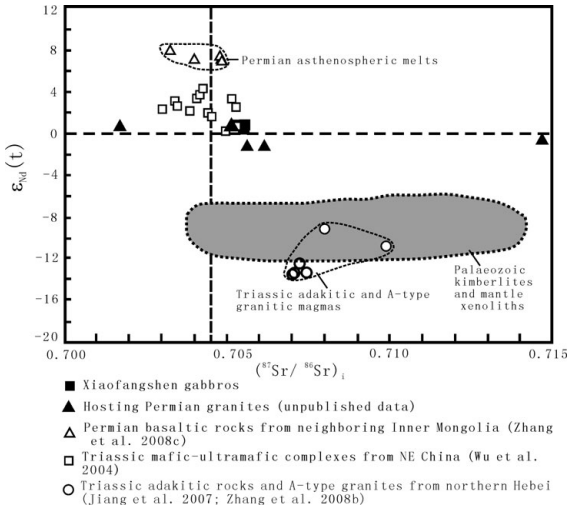

Figure 4. Plot of initial $\varepsilon_{Nd}(t)$ and $(^{87}Sr/^{86}Sr)_i$ for the Xiaofangshen gabbros. The field for the Palaeozoic kimberlites and mantle xenoliths from the eastern North China craton are from Wu *et al.* (2006). Data for the hosting Permian granite (our unpub. data), post-collisional asthenospheric melt as represented by Permian basaltic rocks from neighbouring Inner Mongolia (Zhang *et al.* 2008*c*), Triassic mafic–ultramafic complexes from NE China (Wu *et al.* 2004) and early Triassic adakitic rocks and A-type granites from northern Hebei (Jiang *et al.* 2007; Zhang *et al.* 2008*b*) are included for comparison.

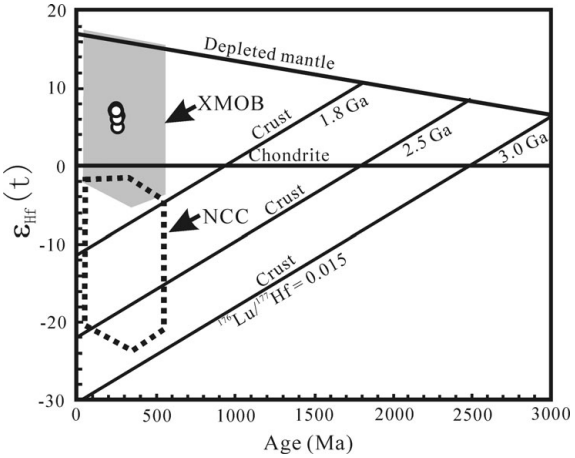

Figure 5. U–Pb age v. Initial epsilon Hf for zircons from the Xiaofangshen gabbros. The fields for the Xing-Meng orogenic belt and North China craton are from Yang *et al.* (2006). NCC – North China craton; XMOB – Xing-Meng orogenic belt.

Table 4. Hf isotope analyses of zircons from the Xiaofangshen gabbros (sample Fk04-5)

Spot	$^{176}Yb/^{177}Hf$	$^{176}Lu/^{177}Hf$	$^{176}Hf/^{177}Hf$	2σ	Hf	ε_{Hf} (0)	ε_{Hf} (t)	T^{Hf}_{DM} (Ma)	$T_{DM}{}^{C}$ (Ma)
01	0.021487	0.000899	0.282818	0.000018	0.282814	1.6	6.8	613	839
02	0.017403	0.000958	0.282826	0.000016	0.282822	1.9	7.1	603	822
03	0.011157	0.000494	0.282821	0.000016	0.282819	1.7	7.3	603	828
04	0.008148	0.000385	0.282789	0.000018	0.282787	0.6	5.8	646	900
05	0.005567	0.000264	0.282815	0.000015	0.282814	1.5	6.8	607	840
06	0.012215	0.000536	0.282756	0.000017	0.282753	−0.6	4.6	694	976
07	0.025914	0.001098	0.282809	0.000017	0.282804	1.3	6.4	630	862
08	0.005313	0.000245	0.282793	0.000016	0.282792	0.7	6.0	638	889
09	0.024944	0.001045	0.282823	0.000019	0.282818	1.8	6.9	609	830

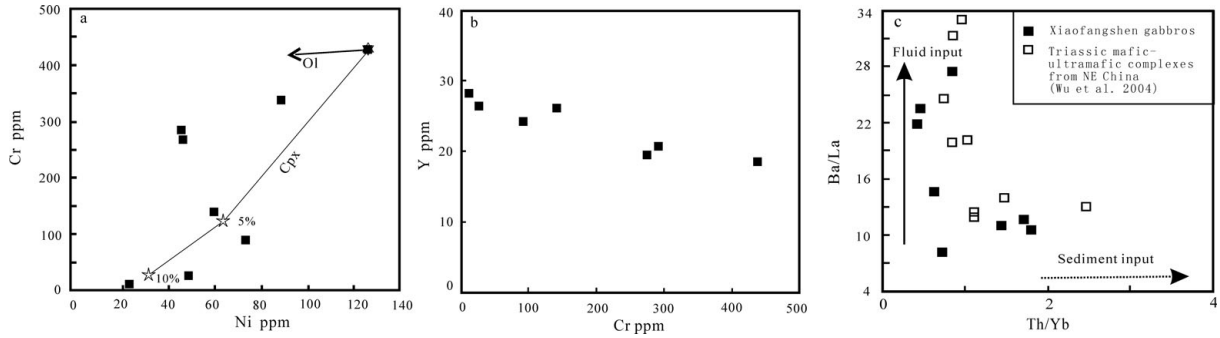

Figure 6. (a) Cr v. Ni, (b) Y v. Cr and (c) Ba/La v. Th/Yb plots for the Xiaofangshen gabbros. In (a), direction of fractionation vectors for olivine and clinopyroxene separation from a relatively primitive sample are based on partition coefficients from Rollinson (1993). The olivine vector is not quantified due to uncertainties concerning the appropriate olivine–basaltic liquid Kd for Ni. In (c), continuous vector – slab-derived fluids; dashed vector – sediment input in the source as represented and discussed by Woodhead *et al.* (2001).

Furthermore, as is usually the case for the mantle-derived magmas erupted in a continental setting, crustal contamination would have been involved in the genesis of the Xiaofangshen gabbros. However, given their higher Sr abundances (487–772 ppm) than those of continental crust (Sr = 280–348 ppm: Rudnick & Gao, 2003) and the hosting Permian granite (Sr = 35.1–114 ppm; our unpub. data: Appendix Table 1, available online as supplementary material at http://www.cambridge.org/journals/geo), and the nearly consistent Sr–Nd isotopic compositions, crustal contamination seems to be insignificant. As such, the elemental and isotopic signatures of the Xiaofangshen gabbros were mainly inherited from those of parental mantle sources, and we thus can use the assumed most primitive samples to probe their mantle sources.

Petrographically, the hornblende-rich character of the Xiaofangshen gabbros is reminiscent of that of the high-level hornblende-rich mafic intrusions from the Mesozoic Sierra Nevada batholith (Sisson, Grove & Coleman, 1996), indicating that their parental magma was rich in H_2O and arguably was derived from an arc-modified source mantle. This suggestion is further supported by their trace element systematics. As widely documented (e.g. Stern, 2002), the enrichment in large ion lithophile elements and light REE and depletion in high field strength elements (e.g. Nb, Ta, Zr and Ti) are typical of subduction-related magmatism. High La/Nb (2.46–4.01), Ba/Nb(22–73) and Zr/Nb ratios (8.8–21.8) in the Xiaofangshen gabbros bear close resemblance to those of arc volcanic rocks worldwide (Wang *et al.* 2005). According to the chromatographic model proposed by Stein, Navon & Kessel (1997) for the transport of trace elements in the mantle wedge, the upper zones in the chromatographic column will be enriched in the incompatible and mobile elements such as Rb, Pb and LREE. The slight enrichment of the Xiaofangshen mafic magmas in Rb/Sr and Nd/Sm, as reflected by their isotopic ratios, is consistent with their derivation from such an enriched part of the lithosphere. This scenario is also consistent with the relatively flat MREE to HREE patterns (Fig. 3a) of the Xiaofangshen gabbros, with Yb_N values ranging from 9.76 to 23.4, implying their derivation from partial melting of a transitional mantle source between spinel and garnet stability fields, at a depth of 60–80 km (Watson & McKenzie, 1991).

In general, the Ba/La fractionation can only be reasonably achieved by elemental mobility in hydrous fluids (McCulloch & Gamble, 1991), whereas Th and LREE are thought to be less mobile in aqueous fluids than the large ion lithophile elements (Pearce *et al.* 1999). As a result, these variables can serve as reliable indicators of potential sediment or fluid contributions to magma source regions (Woodhead *et al.* 2001). Figure 6c suggests that this contribution mainly comes from subduction-derived fluids.

To quantitatively evaluate the melting conditions, we adopted the standard non-modal batch melting equations of Shaw (1970) to model the REE patterns of the Xiaofangshen gabbros with K_D values from Gorring & Kay (2001). Modelling parameters, mantle source composition, melt and source mode, and the degree of partial melting are listed in Table 5. Concentrations of REE in the peridotitic source are assumed to be 1.3 times primitive mantle of Sun & McDonough (1989). With their relatively high Mg no. (59.2–67.6) and Cr (291–438 ppm) abundances, the most primitive samples Fk04-5, Fk06-4 and Fk06-12 can be approximated as the primary melt (or minimally modified melt). For samples Fk04-5 and Fk06-4 with Yb_N values of 9.76 and 10.79, the melting model is based on a starting assemblage of spinel–garnet peridotite. The best-fit REE patterns correspond to a melt fraction of 4.5–6.3 % (Table 5, Fig. 7). In the case of sample Fk06–12 with an Yb_N value of 23.39, the melting model is based on a spinel-bearing peridotite (0.50Ol + 0.23Opx + 0.25Cpx + 0.02Sp) as starting assemblage. The best-fit REE pattern corresponds to a melt fraction of 1.5 % (Table 5, Fig. 7).

The Sr, Nd and Hf isotopic data of the Xiaofangshen gabbros may provide further information on the nature of their source region. As shown above, the Xiaofangshen gabbros exhibit moderate initial $^{87}Sr/^{86}Sr$ ratios (0.7053–0.7055) and slightly positive $\varepsilon_{Nd}(t)$

Table 5. Model parameters and results of non-modal batch partial melting calculations (ppm)

Sample	Fk06-4	Fk04-5	Fk06-12	Sample	Fk06-4	Fk04-5	Fk06-12
Phase	Source mode			Phase	Melt mode		
Olivine	0.5	0.44	0.5	Olivine	0.35	0.25	0.25
Opx	0.17	0.14	0.23	Opx	0.25	0.25	0.25
Cpx	0.27	0.37	0.25	Cpx	0.15	0.2	0.2
Spinel	0.02	0.01	0.02	Spinel	0.25	0.2	0.3
Garnet	0.04	0.04	0	Garnet	0	0.1	0

	Best fit to			Source	Partition coefficients				
REE	Fk06-4	Fk04-5	Fk06-12	S	Ol	Opx	Cpx	Sp	Grt
La	14.99	10.69	31.49	0.89	0.000007	0.0005	0.0536	0.0006	0.01
Ce	33.65	24.171	63.37	2.31	0.00001	0.0009	0.0858	0.0006	0.021
Nd	17.73	13.041	27.79	1.76	0.00007	0.009	0.1873	0.0006	0.087
Sm	4.31	3.2425	6.29	0.58	0.0007	0.02	0.291	0.0006	0.217
Eu	1.43	1.0974	2.11	0.22	0.00095	0.03	0.3288	0.0006	0.4
Gd	4.49	3.5103	6.72	0.77	0.0012	0.04	0.367	0.0006	0.6
Dy	4.26	3.4879	6.86	0.96	0.004	0.06	0.442	0.0015	1.3
Ho	0.86	0.735	1.58	0.21	0.0065	0.065	0.4145	0.0023	2
Er	2.21	1.9777	4.77	0.62	0.009	0.07	0.387	0.003	3
Yb	1.85	1.7084	4.13	0.64	0.023	0.1	0.43	0.0045	4.03
Lu	0.27	0.2483	0.56	0.10	0.035	0.15	0.433	0.0045	4.03

Sources: S – 1.3 times primitive mantle of Sun & McDonough (1989); source and melt mineralogy are taken arbitrarily, but similar to those used in other partial melting calculations (McKenzie & O'Nions, 1995; Tang *et al.* 2006).

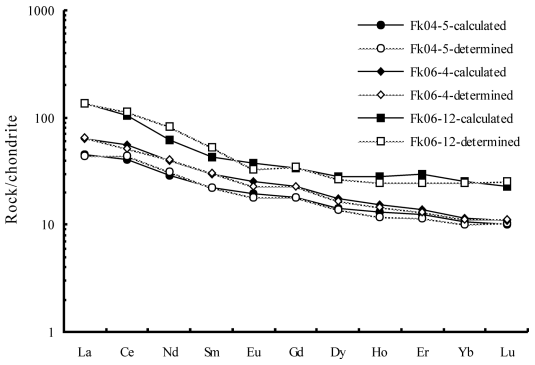

Figure 7. Chondrite-normalized REE patterns for the determined values and the non-modal batch melting model results for the Xiaofangshen gabbros.

values (+0.40 – +0.68). This is similar to those of the late Triassic Hongqiling mafic–ultramafic complexes from the Xing-Meng orogenic belt (Fig. 4; Wu *et al.* 2004), but is distinctive from those of Archaean to Palaeoproterozoic subcontinental lithospheric mantle beneath the northern margin of the eastern North China craton during late Palaeozoic to early Mesozoic times (Wu *et al.* 2006; Zhang *et al.* 2008*a*). Moreover, on the $\varepsilon_{Hf}(T)$ v. emplacement age plot (Fig. 5), all zircon points plot into the field of the Xing-Meng orogenic belt, as defined by the igneous zircons extracted from Phanerozoic granites and volcanic rocks in the Xing-Meng orogenic belt (Yang *et al.* 2006). Therefore, both the positive whole-rock $\varepsilon_{Nd}(t)$ values and young Nd model ages and the highly positive zircon $\varepsilon_{Hf}(T)$ values and young Hf model ages suggest that the parental magma for the Xiaofangshen gabbros likely originated from the juvenile lithospheric mantle that has an affinity with the Xing-Meng orogenic belt.

6.b. Tectonic implications

As outlined in the introduction, the tectonic affinity of the Faku dome has been a controversial but important issue, given its critical locality between a Phanerozoic accretionary orogen and a Precambrian craton. Our previous zircon U–Pb and other mineral $^{40}Ar/^{39}Ar$ dating on the deformed felsic intrusive rocks, which were once regarded as the Precambrian crystalline basement, reveals that they actually were crustal level records of the Permian to early Triassic magmatic and tectonic events (Zhang, Wang & Li, 2005; Zhang, Su & Wang, 2005). These late Palaeozoic to early Mesozoic ages lead us to suggest that no large-scale Precambrian crystalline basement existed in the Faku dome. This echoes the similar suggestions for the basement nature in regions such as the Xing'an block (Miao *et al.* 2003), the Songliao Basin (Wu *et al.* 2004; Pei *et al.* 2007) and the Jiamusi Block (Wilde, Wu & Zhang, 2003).

The occurrence of the Xiaofangshen mafic rocks suggests that a juvenile lithospheric mantle with an affinity with the Xing-Meng orogenic belt existed in the Faku area during early Mesozoic times. This is consistent with the contrast in lithospheric structure revealed by systematic geological–geophysical sections: Western Liaoning is characterized by a thick lithosphere with high rigidity and strength, whereas Songliao and northern Liaoning are characterized by relatively thin lithosphere with low rigidity and strength (Xu *et al.* 2000).

Such mantle- and crustal-level coherence implies that the northern Liaoning block has a tectonic affinity with the Phanerozoic accretionary orogenic belt. This revelation provides an important constraint on the suggestion that the surface suture between the North China Craton and the Xing-Meng orogenic belt in northern Liaoning is located along the

Chifeng–Kaiyuan fault, but not the Xilamulunhe fault as previously advocated.

As widely documented, the Solonker zone has been regarded as the site of final closure of the Palaeo-Asian ocean (e.g. Tang, 1990; Şengör, Natal'in & Burtman, 1993; Xiao *et al.* 2003). There exists much controversy concerning the timing of its suturing. Some authors propose that the suturing took place during Permian to early Triassic times (Şengör, Natal'in & Burtman, 1993; Chen *et al.* 2000; Xiao *et al.* 2003), whereas some authors prefer suturing during either the middle Devonian epoch (Tang, 1990) or late Devonian to early Carboniferous times (Shao, 1991; Hong *et al.* 1995); still others advocate a middle Mesozoic suturing time based on a controversial amphibole K–Ar age (Nozaka & Liu, 2002). However, our recent documentation of the early Permian post-collisional bimodal volcanism along central Inner Mongolia suggests that the North China craton and Mongolian microcontinents amalgamated by early Permian times, and this resulted in the Mesozoic North China–Mongolian Plate (Zhang *et al.* 2008*c*). The widespread occurrence of the Late Permian–Middle Triassic post-orogenic intrusive suites along the western segment of the northern margin of the North China craton echoes this suggestion (Zhang *et al.* 2008*b*).

As reviewed by various authors (e.g. Liegeois, 1998; Vanderhaeghe & Teyssier, 2001; Bonin, 2004), an orogenic cycle typically features a pre-collisional period characterized by subduction, leading to oceanic basin closure and terrane docking, a period of arc–continent or continent–continent collision accommodated by crustal thickening, post-collisional, post-orogenic and within-plate anorogenic episodes. The corresponding four stages of the mantle unrooting process are identified as orogenic growth, initiation of gravitational instability until lithospheric failure, sinking of the detached lithosphere and relaxation of the system (Marotta, Fernandez & Sabadini, 1998).

When evaluated within this general context of thermal and mechanical evolution of the continental crust during orogenesis, the northern margin of the newly amalgamated North China–Mongolian Plate was tectonically dominated by post-orogenic to within-plate anorogenic extensional regimes during early–middle Triassic times, possibly corresponding to a transitional regime from the third to fourth stage, that is, lithosphere delamination and subsequent relaxation, in terms of the mantle unrooting process (Marotta, Fernandez & Sabadini, 1998).

During this pivotal period, repetitive generation of water-bearing magmas resulted in an increasingly depleted and dehydrated continental lithosphere (Bonin, 2004). This led to the thermal and mechanical instability of the thickened lithosphere keel and, coupled with the weak link with the crust (Meissner & Mooney, 1998), induced delamination of the subcontinental lithospheric mantle and subsequent crustal extension (Marotta, Fernandez & Sabadini, 1998). This extensional tectonic regime enables rapid upwelling of asthenosphere, and triggers concomitant decompressional partial melting of the mantle and the magmatic underplating at the crust–mantle boundary. Upon the complete amalgamation of continental terranes, the juvenile within-plate subcontinental lithosphere grows with time by cooling and by continued underplating of deeper materials (Bonin, 2004).

It was such a favourable scenario that led to the formation of the middle Triassic Xiaofangshen gabbros, the early Triassic adakitic rocks (Jiang *et al.* 2007) and A-type granites (Zhang *et al.* 2008*b*) from the northern Hebei area, the Triassic Fanshan ultramafic complex dating from 218 to 243 Ma (Mu *et al.* 2001; Jiang *et al.* 2004) and the Triassic cumulate and granulite xenoliths dating from 220 to 251 Ma from Chifeng of the southern Inner Mongolia (Shao *et al.* 1999; Shao, Han & Li, 2000). Dehydration of the thinning lithosphere resulted ultimately in the shift in a few million years from calc-alkaline to alkaline magmatic suites, as indicated by the Triassic alkaline intrusions dating from 205 to 250 Ma within the continental interior of the newly amalgamated North China–Mongolian Plate (Shao, Mu & Zhang, 2000; Yan *et al.* 2000).

7. Conclusions

(1) SHRIMP U–Pb zircon dating and geochemical analyses document an episode of middle Triassic mafic magmatism in the Faku dome of the northern Liaoning area at the northern margin of the North China–Mongolian plate, as represented by the Xiaofangshen gabbros. Their hornblende-rich character and typical geochemical signatures argue for an origin that is consistent with a small amount of partial melting of a subduction metasomatized lithospheric mantle.

(2) The juvenile character of both the lithospheric mantle and crustal levels suggests that the northern Liaoning block has a tectonic affinity with the Phanerozoic accretionary orogenic belt. This revelation indicates that the Chifeng–Kaiyuan fault likely represents the Mesozoic lithospheric boundary between the North China Craton and the Xing-Meng orogenic belt in the northern Liaoning area.

(3) The Xiaofangshen gabbros, together with the Triassic cumulate and granulite xenoliths and the Triassic alkaline intrusions, constitute an important post-orogenic to within-plate anorogenic magmatic province within the continental interior of the newly amalgamated, Mesozoic North China–Mongolian Plate.

Acknowledgements. This study was financially supported by the Knowledge Innovation Program of the Chinese Academy of Sciences (Grant no. KZCX2-YW-103), the Major State Basic Research Program of the People's Republic of China (Grant no. 2006CB403504) and the National Natural Science Foundation of China (Grant nos 40534022 and 40873026). The authors thank Mr H. Li and Ms X. D. Jin in major- and trace-element analysis, and Dr C. F. Li in Sr–Nd isotope analyses. We are also grateful to Dr D. Pyle, Dr B. Chen and one anonymous review for their constructive

suggestions and Mrs J. Holland for editorial handling. This is The Institute for Geoscience Research (TIGeR) publication no. 120.

References

BIRD, P. 1979. Continental delamination and the Colorado Plateau. *Journal of Geophysical Research* **84**, 7561–71.

BLICHERT-TOFT, J. & ALBAREDE, F. 1997. The Lu–Hf isotope geochemistry of chondrites and the evolution of the mantle–crust system. *Earth and Planetary Science Letters* **148**, 243–58.

BONIN, B. 2004. Do coeval mafic and felsic magmas in post-collisional to within-plate regimes necessarily imply two contrasting, mantle and crustal, sources? A review. *Lithos* **78**, 1–24.

CHEN, B., JAHN, B. M., WILDE, S. A. & XU, B. 2000. Two contrasting Palaeozoic magmatic belts in northern Inner Mongolia, China: petrogenesis and tectonic implications. *Tectonophysics* **328**, 157–82.

DAVIES, J. H. & VON BLANCKENBURG, F. 1995. Slab breakoff: a model of lithosphere detachment and its test in the magmatism and deformation of collisional orogens. *Earth and Planetary Science Letters* **129**, 85–102.

DAVIS, G. A., ZHENG, Y., WANG, C., DARBY, B. J., ZHANG, C. & GEHRELS, G. E. 2001. Mesozoic tectonic evolution of the Yanshan fold and thrust belt, with emphasis on Hebei and Liaoning provinces, northern China. In *Paleozoic and Mesozoic tectonic evolution of central and eastern Asia: From continental assembly to intracontinental deformation* (eds M. S. Hendrix & G. A. Davis), pp. 171–97. Geological Society of America, Memoir no. 194.

DEWEY, J. F. 1988. Extensional collapse of orogens. *Tectonics* **7**, 1123–39.

ENGLAND, P. & HOUSEMAN, G. 1989. Extension during continental convergence, with application to the Tibetan Plateau. *Journal of Geophysical Research* **94**, 17561–79.

FURLONG, K. P. & FOUNTAIN, D. M. 1986. Continental crustal underplating: thermal consideration and seismic–petrologic consequences. *Journal of Geophysical Research* **91**, 8285–94.

GORRING, M. L. & KAY, S. M. 2001. Mantle processes and sources of Neogene slab window magmas from southern Patagonia, Argentina. *Journal of Petrology* **42**, 1067–94.

GRIFFIN, W. L., WANG, X., JACKSON, S. E., PEARSON, N. J., O'REILLY, S. Y., XU, X. S. & ZHOU, X. M. 2002. Zircon chemistry and magma mixing, SE China: in situ analysis of Hf isotopes, Tonglu and Pingtan igneous complexes. *Lithos* **61**, 237–69.

GU, L., ZHENG, Y., TANG, X., ZAW, K., DELLE-PASQUE, F., WU, C., TIAN, Z., LU, J., NI, P., LI, X., YANG, F. & WANG, X. 2007. Copper, gold and silver enrichment in ore mylonites within massive sulphide orebodies at Hongtoushan VHMS deposit, NE China. *Ore Geology Reviews* **30**, 1–29.

HONG, D. W., HUANG, H. Z., XIAO, Y. J., XU, H. M. & JIN, M. Y. 1995. Permian alkaline granites in central Inner Mongolia and their geodynamic significance. *Acta Geologica Sinica* **8**, 27–39.

JAHN, B. M., WU, F. & CHEN, B. 2000. Granitoids of the Central Asian Orogenic Belt and continental growth in the Phanerozoic. *Transactions of the Royal Society Edinburgh, Earth Sciences* **91**, 181–93.

JIANG, N., CHU, X., MIZUTA, T., ISHIYAMA, D. & MI, J. 2004. A magnetite–apatite deposit in the Fanshan alkaline ultramafic complex, Northern China. *Economic Geology* **99**, 397–408.

JIANG, N., LIU, Y. S., ZHOU, W. G., YANG, J. H. & ZHANG, S. Q. 2007. Derivation of Mesozoic adakitic magmas from ancient lower crust in the North China craton. *Geochimica et Cosmochimica Acta* **71**, 2591–608.

KAY, R. W. & KAY, M. S. 1993. Delamination and delamination magmatism. *Tectonophysics* **219**, 177–89.

LEAKE, B. E., WOOLLEY, A. R., ARPS, C. E. S., BIRCH, W. D., GILBERT, M. C., GRICE, J. D., HAWTHORNE, F. C., KATO, A., KISCH, H. J., KRIVOVICHEV, V. G., LINTHOUT, K., LAIRD, J., MANDARINO, J. A., MARESCH, W. V., NICKEL, E. H., ROCK, N. M. S., SCHUMACHER, J. C., SMITH, D. C., STEPHENSON, N. C. N., UNGARETTI, L., WHITTAKER, E. J. W. & YOUZHI, G. 1997. Nomenclature of amphiboles: report of the subcommittee on amphiboles of the international mineralogical association, Commission on new minerals and mineral names. *American Mineralogist* **82**, 1019–37.

LE MAITRE, R. W. 2002. *Igneous rocks: a Classification and Glossary of Terms*, 2nd edition. Cambridge: Cambridge University Press, 236 pp.

LIAONING BUREAU OF GEOLOGY AND MINERAL RESOURCES. 1989. *Regional Geology of Liaoning Province*. Beijing: Geological Publishing House, 856 (in Chinese).

LIAONING BUREAU OF GEOLOGY AND MINERAL RESOURCES. 1998. *1:50000 scale regional geology of the Faku, Wutaizi, and Daming, Liaoning Province*. Beijing: Geological Publishing House (in Chinese).

LIÉGEOIS, J. 1998. Preface – some words on the post-collisional magmatism. *Lithos* **45**, XV–XVII.

LIU, D., NUTMAN, A. P., COMPSTON, W., WU, J. & SHEN, Q. 1992. Remnants of 3800 Ma crust in the Chinese part of the Sino-Korean craton. *Geology* **20**, 339–42.

LUDWIG, K. 2001. *User manual for isoplot/EX (2.49)*. Berkeley Geochronology Center, Special Publication no. 1a. 55 pp.

LUGMAIR, G. W. & HARTI, K. 1978. Lunar initial $^{143}Nd/^{144}Nd$: differential evolution of the lunar crust and mantle. *Earth and Planetary Science Letters* **39**, 349–57.

MAROTTA, A. M., FERNANDEZ, M. & SABADINI, R. 1998. Mantle unrooting in collisional setting. *Tectonophysics* **296**, 31–46.

MCCULLOCH, M. T. & GAMBLE, J. A. 1991. Geochemical and geodynamical constraints on subduction zone magmatism. *Earth and Planetary Science Letters* **102**, 358–74.

MCKENZIE, D. & O'NIONS, R. K. 1995. The source regions of oceanic island basalts. *Journal of Petrology* **36**, 133–59.

MEISSNER, R. & MOONEY, W. 1998. Weakness of the lower continental crust: a condition for delamination, uplift and escape. *Tectonophysics* **296**, 47–60.

MENG, Q. & ZHANG, G. 2000. Geological framework and tectonic evolution of Qinling orogen, central China. *Tectonophysics* **323**, 183–96.

MIAO, L. C., FAN, W., ZHANG, F., LIU, D., JIAN, P., SHI, G., TAO, H. & SHI, Y. 2003. Zircon SHRIMP geochronology of the Xinkailing–Kele complex in the northwestern Lesser Xing'an Range, and its geological implications. *Chinese Science Bulletin* **48**, 2315–23.

MU, B., SHAO, J., CHU, Z., YAN, G. & QIAO, G. 2001. Sm–Nd age and Sr, Nd isotopic characteristics of the Fanshan potassic alkaline ultramafic syenitic complex in Hebei Province, China. *Acta Petrologica Sinica* **17**, 358–65.

NOZAKA, T. & LIU, Y. 2002. Petrology of the Hegenshan ophiolite and its implications for the tectonic evolution of northern China. *Earth and Planetary Science Letters* **202**, 89–104.

PEARCE, J. A., KEMPTON, P. D., NOWELL, G. M. & NOBLE, S. R. 1999. Hf–Nd element and isotope perspective on

the nature and provenance of mantle and subduction components in western Pacific arc–basin systems. *Journal of Petrology* **11**, 1579–1611.

PEI, F. P., XU, W. L., YANG, B. B., ZHAO, Q. G., LIU, X. M. & HU, Z. C. 2007. Zircon U–Pb geochronology of basement metamorphic rocks in the Songliao Basin. *Chinese Science Bulletin* **52**, 942–8.

ROLLINSON, H. R. 1993. *Using geochemical data: evaluation, presentation, interpretation*. Singapore: Longman.

RUDNICK, R. L. & GAO, S. 2003. Composition of the continental crust. In *The Crust, Treatise in Geochemistry*, vol. 3 (ed. R. L. Rudnick), pp. 1–64. Oxford: Elsevier-Pergamon.

RUPPEL, C. 1995. Extensional processes in continental lithosphere. *Journal of Geophysical Research* **100**, 24187–215.

ŞENGÖR, A. M. C., NATAL'IN, B. A. & BURTMAN, V. S. 1993. Evolution of the Altaid tectonic collage and Palaeozoic crustal growth in Eurasia. *Nature* **364**, 299–307.

SHAO, J. A. 1991. *Crust evolution in the middle part of the northern margin of Sino-Korean plate*. Beijing: Publishing House of Peking University.

SHAO, J., HAN, Q., ZHANG, L. & MU, B. 1999. Cumulate complex xenoliths in the early Mesozoic in eastern Inner Mongolia. *Chinese Science Bulletin* **44**, 1272–9.

SHAO, J., HAN, Q. & LI, H. 2000. Discovery of the Early Mesozoic granulite xenoliths in North China Craton. *Science in China* (Series D) **43**, 245–52.

SHAO, J., MU, B. & ZHANG, L. 2000. Deep geological process and its shallow response during Mesozoic transfer of tectonic framework in eastern North China. *Geological Review* **46**, 32–40.

SHAW, D. M. 1970. Trace element fractionation during anatexis. *Geochimica et Cosmochimica Acta* **34**, 237–43.

SISSON, T. W., GROVE, T. L. & COLEMAN, D. S. 1996. Hornblende gabbro sill complex at Onion Valley, California, and a mixing origin for the Sierra Nevada batholith. *Contributions to Mineralogy and Petrology* **126**, 81–108.

SODERLUND, U., PATCHETT, P. J., VERVOORT, J. D. & ISACHSEN, C. E. 2004. The ^{176}Lu decay constant determined by Lu–Hf and U–Pb isotope systematics of Precambrian mafic intrusions. *Earth and Planetary Science Letters* **219**, 311–24.

STEIGER, R. H. & JÄGER, E. 1977. Subcommission on geochronology; convention on the use of decay constants in geochronology and cosmochronology. *Earth and Planetary Science Letters* **36**, 359–62.

STEIN, M., NAVON, O. & KESSEL, R. 1997. Chromatographic metasomatism of the Arabian–Nubian lithosphere. *Earth and Planetary Science Letters* **152**, 75–91.

STERN, R. J. 2002. Subduction zones. *Reviews of Geophysics* **40**, 1–38.

SUN, S. S. & MCDONOUGH, W. F. 1989. Chemical and isotopic systematics of oceanic basalts: implications for mantle composition and processes. In *Magmatism in the Ocean Basins* (eds A. D. Saunders & M. J. Norry), pp. 528–48. Geological Society of London, Special Publication no. 42.

TANG, K. 1990. Tectonic development of Paleozoic fold belts at the north margin of the Sino-Korean Craton. *Tectonics* **9**, 249–60.

TANG, Y. J., ZHANG, H. F. & YING, J. F. 2006. Asthenosphere–lithospheric mantle interaction in an extensional regime: implication from the geochemistry of Cenozoic basalts from Taihang Mountains, North China Craton. *Chemical Geology* **233**, 309–27.

VANDERHAEGHE, O. & TEYSSIER, C. 2001. Partial melting and flow of orogens. *Tectonophysics* **342**, 451–72.

WANG, Y. J., FAN, W. M., PENG, T. P., ZHANG, H. F. & GUO, F. 2005. Nature of the Mesozoic lithospheric mantle and tectonic decoupling beneath the Dabie orogen, central China: evidence from Ar–Ar geochronology, elemental and Sr–Nd–Pb isotopic compositions of early Cretaceous mafic rocks. *Chemical Geology* **220**, 165–89.

WATSON, S. & MCKENZIE, D. 1991. Melt generation by plumes: A study of Hawaiian volcanism. *Journal of Petrology* **32**, 501–37.

WILDE, S. A., WU, F. Y. & ZHANG, X. Z. 2003. Late Pan-African magmatism in northeastern China: SHRIMP U–Pb zircon evidence from granitoids in the Jiamusi Massif. *Precambrian Research* **295**, 1–17.

WILLIAMS, I. S. 1998. U–Th–Pb geochronology by ion microprobe. In *Applications of microanalytical techniques to understanding mineralizing processes* (eds M. A. McKibben, W. C. Shanks & W. I. Ridley), pp. 1–35. *Reviews in Economic Geology* **7**.

WOODHEAD, J. D., HERGT, J. M., DAVIDSON, J. P. & EGGINS, S. M. 2001. Hafnium isotope evidence for 'conservative' element mobility during subduction zone processes. *Earth and Planetary Science Letters* **192**, 331–46.

WOODHEAD, J. D., HERGT, J., SHELLEY, M., EGGINS, S. & KEMP, R. 2004. Zircon Hf-isotope analysis with an excimer laser, depth profiling, ablation of complex geometries, and concomitant age estimation. *Chemical Geology* **209**, 121–35.

WU, F. Y., WILDE, S. A., ZHANG, G. L. & SUN, D. Y. 2004. Geochronology and petrogenesis of the post-orogenic Cu–Ni sulfide-bearing mafic–ultramafic complexes in Jilin Province, NE China. *Journal of Asian Earth Sciences* **23**, 781–97.

WU, F. Y., WALKER, R. J., YANG, Y. H., YUAN, H. L. & YANG, J. H. 2006. The chemical–temporal evolution of lithospheric mantle underlying the North China Craton. *Geochimica et Cosmochimica Acta* **70**, 5013–34.

XIAO, W., WINDLEY, B. F., HAO, J. & ZHAI, M. 2003. Accretion leading to collision and the Permian Solonker suture, Inner Mongolia, China: Termination of the central Asian orogenic belt. *Tectonics* **22**, 1484–1505.

XU, M., MIDDLETON, M. F., XUE, L. F. & WANG, D. P. 2000. Structure of the Lithosphere and Mesozoic sedimentary basins in Western Liaoning, Northern Liaoning, and Songliao, Northeast China. *International Geology Review* **42**, 269–78.

YAN, G., MU, B., XU, B., HE, G., TAN, L., ZHAO, H. & HE, Z. H. 2000. Geochronology and isotopic features of Sr, Nd, and Pb of the Triassic alkali intrusions in the Yanshan–Yinshan regions. *Science in China* (series D) **30**, 384–7.

YANG, J. H., WU, F. Y., SHAO, J. A., WILDE, S. A., XIE, L. W. & LIU, X. M. 2006. Constraints on the timing of uplift of the Yanshan fold and thrust belt, North China Craton. *Earth and Planetary Science Letters* **246**, 336–52.

YIN, A. & NIE, S. 1996. A Phanerozoic palinspastic reconstruction of China and its neighboring regions. In *Tectonic Evolution of Asia* (eds A. Yin & T. M. Harrison), pp. 442–85. Cambridge University Press.

ZHANG, H. F., GOLDSTEIN, S. L., ZHOU, X. H., SUN, M., ZHENG, J. P. & CAI, Y. 2008*a*. Evolution of subcontinental lithospheric mantle beneath easten China: Re–Os isotopic evidence from mantle xenoliths in Paleozoic kimberlites and Mesozoic basalts. *Contributions to Mineralogy and Petrology* **155**, 271–93.

ZHANG, S. H., ZHAO, Y., SONG, B., HU, J. M., LIU, S.W., YANG, Y. H., CHEN, F. K., LIU, X. M. & LIU, J. 2008*b*. Contrasting Late Carboniferous and Late Permian–Middle Triassic intrusive suites from the northern margin of the North China craton: Geochronology, petrogenesis, and tectonic implications. *Geological Society of America Bulletin* (in press).

ZHANG, X. H., WANG, H. & LI, T. S. 2005. $^{40}Ar/^{39}Ar$ geochronology of the Faku tectonites: Implications for the tectonothermal evolution of the Faku block, northern Liaoning. *Science in China (series D)* **48**(5), 601–12.

ZHANG, X. H., SU, W. J. & WANG, H. 2005. Zircon SHRIMP geochronology of the Faku tectonites in the northern Liaoning province: implications for the northern boundary of the North China craton. *Acta Petrologica Sinica* **21**, 135–42.

ZHANG, X. H., ZHANG, H. F., TANG, Y. J., WILDE, S. A. & HU, Z. C. 2008*c*. Geochemistry of Permian bimodal volcanic rocks from Central Inner Mongolia, North China: Implication for Tectonic setting and Phanerozoic continental growth in Central Asian Orogenic Belt. *Chemical Geology* **249**, 262–81.

ZHAO, G. C., WILDE, S. A., CAWOOD, P. A. & SUN, M. 2001. Archean blocks and their boundaries in the North China craton: lithological, geochemical, structural and P–T path constraints and tectonic evolution. *Precambrian Research* **107**, 45–73.

ZHENG, J. P., GRIFFIN, W. L., O'REILLY, S. Y., LU, F. X., WANG, C. Y., ZHANG, M., WANG, F. Z. & LI, H. M. 2004. 3.6 Ga lower crust in central China: new evidence on the assembly of the North China craton. *Geology* **32**, 229–32.